Earth and Planetary Science Letters 421 (2015) 20–26

Contents lists available at ScienceDirect

Earth and Planetary Science Letters

www.elsevier.com/locate/epsl

Viscosity undulations in the lower mantle: The dynamical role of iron spin transition

J.F. Justo [a,*], G. Morra [b], D.A. Yuen [c,d]

[a] Escola Politécnica, Universidade de São Paulo, CP 61548, CEP 05424-970, São Paulo, SP, Brazil
[b] Department of Physics and School of Geosciences, University of Louisiana at Lafayette, LA 70504, United States
[c] Department of Earth Sciences, University of Minnesota, Minneapolis, MN 55455, United States
[d] School of Environmental Studies, China University of Geosciences, Wuhan, 430074, China

ARTICLE INFO

Article history:
Received 1 October 2014
Received in revised form 4 March 2015
Accepted 5 March 2015
Available online 11 April 2015
Editor: P. Shearer

Keywords:
viscosity
lower mantle
mantle plume
elasticity
spin transition

ABSTRACT

A proper determination of the lower-mantle viscosity profile is fundamental to understanding Earth geodynamics. Based on results coming from different sources, several models have been proposed to constrain the variations of viscosity as a function of pressure, stress and temperature. While some models have proposed a relatively modest viscosity variation across the lower mantle, others have proposed variations of several orders of magnitude. Here, we have determined the viscosity of ferropericlase, a major mantle mineral, and explored the role of the iron high-to-low spin transition. Viscosity was described within the elastic strain energy model, in which the activation parameters are obtained from the bulk and shear wave velocities. Those velocities were computed combining first principles total energy calculations and the quasi-harmonic approximation. As a result of a strong elasticity softening across the spin transition, there is a large reduction in the activation free energies of the materials creep properties, leading to viscosity undulations. These results suggest that the variations of the viscosity across the lower mantle, resulting from geoid inversion and postglacial rebound studies, may be caused by the iron spin transition in mantle minerals. Implications of the undulated lower mantle viscosity profile exist for both, down- and up-wellings in the mantle. We find that a viscosity profile characterized by an activation free energy of $G^*(z_0) \sim 300$–400 kJ/mol based on diffusion creep and dilation factor $\delta = 0.5$ better fits the observed high velocity layer at mid mantle depths, which can be explained by the stagnation and mixing of mantle material. Our model also accounts for the growth of mantle plume heads up to the size necessary to explain the Large Igneous Provinces that characterize the start of most plume tracks.

1. Introduction

Lower mantle viscosity has been the subject of great debate over the last decades (Sammis et al., 1977; Ricard and Wuming, 1991; Forte and Mitrovica, 2001), and its determination would be fundamental to address a number of questions on the mantle, such as its composition, heterogeneity, and geodynamics. Interpretation of data, coming from geoid inversion and postglacial rebound studies, indicated undulations in the viscosity profile, with peaks around 1300 and 2000 km deep and a valley around 1600 km (Mitrovica and Forte, 2004). If viscosity is considered as controlled by thermally activated microscopic mechanisms (Sammis et al., 1977; Ellsworth et al., 1985), this viscosity profile could not be easily reconciled with a single diffusion creep mechanism taking place in the lower mantle. Those variations in the lower mantle viscosity suggest that several microscopic competing diffusion mechanisms could be taking place in the mantle. On the other hand, the recent discovery of the iron spin transition in major mantle minerals (Badro et al., 2003, 2004; Lin et al., 2005, 2007; Speziale et al., 2005; Tsuchiya et al., 2006; Fei et al., 2007), and the corresponding anomalies in their elasticity (Crowhurst et al., 2008; Wentzcovitch et al., 2009; Marquardt et al., 2009; Wu et al., 2009; Antonangeli et al., 2011; Wu and Wentzcovitch, 2014), could reconcile the description of viscosity with a single thermally activated mechanism by using the available information from simultaneous inversion of geoid and post-glacial rebound data (Mitrovica and Forte, 2004).

Van Keken et al. (1992) found that some radial viscosity profile would produce a pulsating diapiric rise. This work has simulated numerous investigations of the effects of non-monotonous

* Corresponding author.
E-mail address: jjusto@lme.usp.br (J.F. Justo).

http://dx.doi.org/10.1016/j.epsl.2015.03.013
0012-821X/

viscosity profile in the lower mantle. Tomographic models of slabs that penetrated in the lower mantle show strong signals of large body lying between 1500 and 2000 km depth (Grand, 1994), such as the Farallon slab (Sigloch et al., 2008). This result has been confirmed by the analysis of a variety of global tomographic models, e.g. Tx2007 (Simmons et al., 2006), Rmsl-s06 (Li et al., 2007), Saw642an (Panning and Romanowicz, 2006), all finding a clear transition from fast to slow shear seismic velocities for degree up to ∼16 at a less than 1500 km depth (Boschi et al., 2008). Morra et al. (2010) showed that a sinking plate might penetrate, reorganize or even stall when crossing a 200 to 500 km high viscosity region in the middle of the lower mantle. Shahnas et al. (2011) used global mantle convection models to demonstrate that the only effects on the density of the iron spin transition enhances the vigor of rising plumes below 2000 km depth and slightly increases the temperature of the lowermost region of the mantle. Peltier and Drummond (2010) used glacial isostatic adjustment observations to infer a modest increase of the viscosity at mid mantle depths. Overall, those investigations have shown that a non-monotonic lower mantle viscosity profile would create substantial complications to the dynamics of sinking slabs and rising plumes. Here, we employ a standard scaling for plume head size evolution (e.g., Griffiths and Campbell, 1990; Ribe et al., 2007) integrating it along a one-dimensional vertical profile to calculate a broad range of solutions for the dynamics of a plume rise through a variety of physically based lower mantle viscosity profiles, obtained by first principles calculations of mineral elasticity.

We used the elastic properties of ferropericlase (Fp), $Mg_{1-x}Fe_xO$ with $x = 0.1875$, computed by a combination of first principles calculations and quasiharmonic approximation (Carrier et al., 2008; Wentzcovitch et al., 2009; Wu et al., 2013), to determine its viscosity under lower mantle conditions. Fp was treated as a solid solution in a mixed spin state, with the concentration of material with iron in high and low spin determined by the respective free energies. Although Fp is only the second most abundant lower mantle mineral, it is likely controlling deformation in the lower mantle (Zerr and Boehler, 1994; Yamazaki and Karato, 2001). This is justified by the fact that Fp is softer than the more abundant ferrosilicate perovskite under the same thermodynamic conditions. The viscosity of Fp was described within the elastic strain model (Sammis et al., 1977; Ellsworth et al., 1985), in which the activation energy parameters were computed along adiabatic (0.3 K/km) (Boehler, 2000) and superadiabatic (1.2 K/km) (da Silva et al., 2000) geotherms. The manuscript explores the role of dilatation and shear microscopic mechanisms (Ellsworth et al., 1985), variations in activation energies at the top of the lower mantle, and the Newtonian character of the mantle. The results show that the variations in Fp elasticity due to the iron spin transition can explain the undulations in the mantle viscosity, such as the viscosity hill about 800 km above the core–mantle boundary (Mitrovica and Forte, 2004).

2. Theoretical models

The viscosity (η) of Fp was described as a thermally activated process, as a result of diffusion of atomic species (Saha et al., 2013),

$$\eta = f(\sigma)\exp\left(\frac{G_e^*}{RT}\right) \tag{1}$$

where G_e^* is the Gibbs free energy of activation and $f(\sigma)$ is a function of stress. For a Newtonian fluid, $f(\sigma)$ is a constant and $G^* = G_e^*$, where G^* is the activation energy of the appropriate dynamical mechanism (Ellsworth et al., 1985). On the other hand, the effective viscosity of a power law fluid of order n is equivalent to the viscosity of a Newtonian fluid with an apparent activation energy $G^* = 2G_e^*/(n+1)$ (Karato, 1981). Here we have considered the mineral as a Newtonian fluid, consistent with assumptions used to determine the lower mantle viscosity experimentally (Mitrovica and Forte, 2004). Therefore, the viscosity at a certain depth z, $\eta(z)$, is given by:

$$\eta(z) = \eta(z_0)\exp\left(\frac{G^*(z)}{RT(z)} - \frac{G^*(z_0)}{RT(z_0)}\right) \tag{2}$$

where $z_0 = 670$ km (the top of the lower mantle), $\eta(z_0)$ and $G^*(z_0)$ are respectively the viscosity and the activation free energy at that reference depth.

The activation energy $G^*(z)$ can be described as a linear combination of energies from pure shear, $G_s^*(z)$, and pure dilatation, $G_D^*(z)$, mechanisms:

$$G^*(z) = \delta G_s^*(z) + (1-\delta)G_D^*(z) \tag{3}$$

where δ is a free parameter ($0 \le \delta \le 1$) that weights the respective contributions. Using the elastic strain energy model, those activation energies for pure shear and dilatation can be calculated in terms of the seismic velocities (Ellsworth et al., 1985),

$$\frac{G_s^*(z)}{G_s^*(z_0)} = \left[\frac{V_s(z)}{V_s(z_0)}\right]^2 \quad \text{and} \quad \frac{G_D^*(z)}{G_D^*(z_0)} = \left[\frac{V_\phi(z)}{V_\phi(z_0)}\right]^2 \tag{4}$$

where $V_s(z)$ and $V_\phi(z)$ are respectively the shear and bulk sound wave velocities at a depth z, which were computed from the mineral elastic constants (Wentzcovitch et al., 2009; Wu et al., 2013).

This model has five free parameters: δ, n, $G_s^*(z_0)$, $G_D^*(z_0)$, and $\eta(z_0)$. We have assumed that $G^*(z_0) = G_s^*(z_0) = G_D^*(z_0)$. Earlier phenomenological considerations (Ellsworth et al., 1985) have suggested $G^*(z_0) = 680$ kJ/mol at the top of the lower mantle. However, recent investigations have indicated considerably lower values for this activation energy, around 300 kJ/mol (Stretton et al., 2001; Van Orman et al., 2003; Ito and Tomiuri, 2007). We considered several values for this parameter, ranging from 200 to 500 kJ/mol. The competition between shear and dilatation mechanisms in the lower mantle is still not fully understood, such that we considered values for δ ranging from pure shear to pure dilatation.

According to Eqs. (2)–(4), the viscosity can be computed knowing the shear and bulk sound wave velocities as a function of depth. First of all, we considered adiabatic (≈0.3 K/km) and superadiabatic (≈1.2 K/km) geotherms, allowing explore variations in viscosity for different mantle temperature profiles. In order to compute the seismic velocities, we need the adiabatic bulk $K_s(z)$ and shear $\mu(z)$ moduli and the density $\rho(z)$ of Fp as a function of depth along a geotherm, which requires those properties as a function of pressure and temperature: $K_s(P,T)$, $\mu(P,T)$ and $\rho(P,T)$. In order to obtain those properties, a thermodynamic model to describe the Fp in a mixed spin state was recently developed (Wu et al., 2009, 2013). Within that model, the material, at finite temperatures and pressures, was described as a solid solution in thermal equilibrium, composed of concentrations of iron atoms in low and high spins. The high temperature properties in pure spin states were computed by a combination of first principles calculations and the quasiharmonic approximation (Carrier et al., 2008; Wentzcovitch et al., 2009). The first principles calculations were performed using a plane-wave-pseudopotential methodology in which the electron–electron interactions were described by an invariant version of the local density approximation plus Hubbard potential (LDA+U) (Cococcioni and de Gironcoli, 2005).

In modeling plume upwelling, we follow a standard theory (e.g., Griffiths and Campbell, 1990; Ribe et al., 2007) which relates the mantle viscosity profile with plume rising speed, plume head volume and plume conduit size. The instability that initiates the plume rises with speed $V = g\Delta\rho a^2/3\eta_0$, where a is the radius

of the nearly spherical plume head. This approximation is generally valid for any rising collection of diapirs with heterogeneities in size distribution (e.g. Morra et al., in press). During its rise the plume head grows at a constant rate due to the feeding flow from the conduit Φ_p plus the entrained flow due to the plume head advection $\Phi_e = 2\pi a U \varepsilon$, where $\varepsilon = \sqrt{2\kappa a/U}$ is the thickness of the boundary layer around the plume head, U is the speed of the flow in the plume conduit and κ the thermal diffusivity. Combining these equations, one obtains a scaling for entrained flow $\Phi_e = 2\pi\sqrt{2}a^{3/2}V^{1/2}\kappa^{1/2} = 2\pi a^{5/2}\sqrt{2\kappa g\Delta\rho/3\eta_0}$ which, by assuming a plume head growth controlled by the entrained flow, relates a plume head volume growth rate $\partial V_{head}/\partial t = 4\pi a^2 \partial a/\partial t = \Phi_e$, and therefore $\partial a/\partial t = \sqrt{a\kappa g\Delta\rho/6\eta_0}$.

Numerically, the calculation of the radius head a and of the rising velocity v are discretized integrating their values from the bottom to the top of the lower mantle. The scheme requires only thermal and viscosity profile. The discrete values a_i, v_i and t_i are calculated at constant depth intervals Δz, that we assumed equal to 5 km. For these 1-D simulations, we employed the following parameter set: $\rho = 5000$ kg/m^3, $\alpha = 5\times10^{-5}$ K^{-1}, $\kappa = 10^{-6}$ m^2/s, $g = 10$ m/s^2. We varied two parameters, ΔT and a_0, the first among three values (150 K, 300 K, 450 K), and a_0, the initial plume head radius, among ten values (50 km to 150 km, every 10 km). At every depth the scheme requires 6 steps:

(i) $\Delta\rho = \rho\alpha\Delta T$;
(ii) $v_{i+1} = g\Delta\rho a_i^2/3\eta_i$;
(iii) $\Delta t = \Delta z/v_{i+1}$;
(iv) $da/dt = a_i\kappa g\Delta\rho/6\eta_i$;
(v) $a_{i+1} = a_i + (da/dt)\,\Delta t$;
(vi) $t_{i+1} = t_i + \Delta t$.

The merit of this simple approach is that we can carry out a detailed parameter space search and learn easily about the main physics of the problem.

3. Viscosity of ferropericlase

Fig. 1 shows the adiabatic bulk and shear moduli and the respective sound wave velocities of Fp along two geotherms. The spin transition causes strong softening in the bulk modulus, but minor effect in the shear modulus. These results are consistent with recent experimental data on the elasticity of ferropericlase (Marquardt et al., 2009). The figure shows that the softening is more noticeable in the adiabatic geotherm than in the superadiabatic one. This is because the depth regions in which the spin transition takes place, the temperatures along the adiabatic geotherm are considerably lower than the respective ones in the superadiabatic geotherm. The figure also shows the normalized activation parameters of viscosity as a function of depth for dilatation and shear mechanisms, computed according to the elastic strain model (Ellsworth et al., 1985). The activation free energy oscillates considerably, mainly in the case of the dilatation mechanisms, which resulted from the elastic softening in the bulk modulus (Wentzcovitch et al., 2009; Wu et al., 2013).

Fig. 2 shows the normalized Fp viscosity, ranging from pure dilatation to pure shear mechanism for two different geotherms, with $G^*(z_0) = 300$ kJ/mol and $n = 1$. The viscosity along the adiabatic geotherm presents strong undulations in the middle of the lower mantle when the dilatation mechanism is considered, and reproduces qualitatively the viscosity data obtained from geoid inversion and postglacial rebound studies (Mitrovica and Forte, 2004). The Fp viscosity presents strong variations of as much as three orders in magnitude along the geotherm, with peaks around 1100 and 2500 km and a valley around 1600 km. These values agree reasonably well with the observed viscosity peaks in

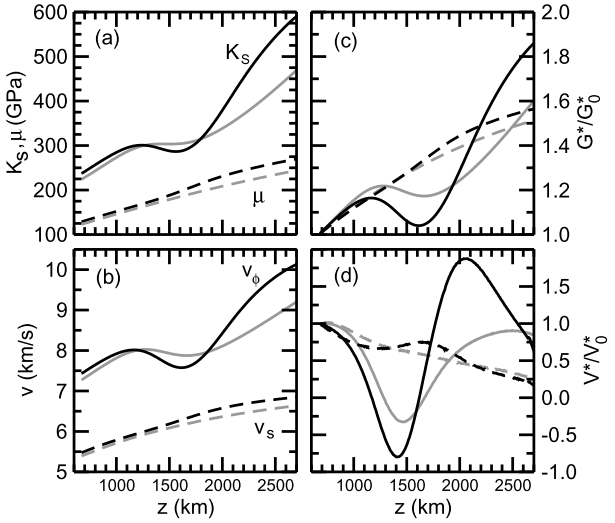

Fig. 1. Calculated (a) adiabatic bulk (full line) and shear (dashed line) moduli and (b) bulk and shear wave velocities of Fp as a function of depth z along two geotherms. The figure also shows the respective (c) activation Gibbs free energy $G^*(z)$ and (d) activation volume $V^*(z)$ normalized with respect to reference values in the top of the lower mantle, $G_0^* = G^*(z_0)$ and $V_0^* = V^*(z_0)$. In (c) and (d), full and dashed lines represent activation parameters for pure dilatation (G_D^* and V_D^*) and pure shear (G_s^* and V_s^*) mechanisms, respectively. Black and gray lines represent results along adiabatic (Boehler, 2000) and superadiabatic (da Silva et al., 2000) geotherms, respectively.

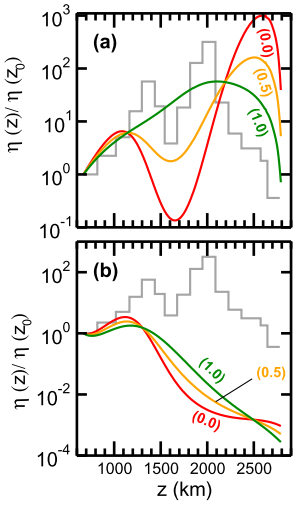

Fig. 2. (Color online.) Calculated normalized Fp viscosity as a function of depth for (a) adiabatic and (b) superadiabatic geotherms for several contributions of dilatation and shear mechanisms. The red, orange and green lines represent respectively $\delta = 0$ (pure dilatation), $\delta = 0.5$, and $\delta = 1.0$ (pure shear). Here, $G^*(z_0) = 300$ kJ/mol and the fluid is considered Newtonian ($n = 1$). The gray line is an estimated normalized viscosity of the lower mantle (Mitrovica and Forte, 2004).

the lower mantle around 1300 and 2000 km and valley around 1600 km (Mitrovica and Forte, 2004). Our results indicate that a single creep mechanism, if connected to the iron spin transition, can lead to undulations in the viscosity. On the other hand, a pure shear mechanism generates only one wide peak in the Fp viscosity, around 2100 km, indicating that dilatation mechanism is important for the viscosity undulations.

The viscosity along the superadiabatic geotherm does not present such undulations, and the viscosity decreases too fast compared to experimental data. This behavior resulted from the high temperatures along the superadiabatic geotherm over the lower mantle, compared to the other geotherm. Along the su-

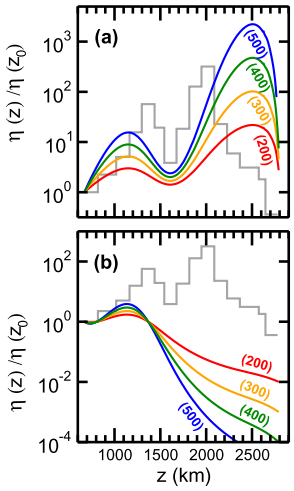

Fig. 3. (Color online.) Calculated normalized Fp viscosity as a function of depth along (a) adiabatic and (b) superadiabatic geotherms for several activation energies in the top of the lower mantle, all with $\delta = 0.5$ and $n = 1$. The red, orange, green, and blue lines represent $G^*(z_0)$ respectively 200, 300, 400, and 500 kJ/mol. The gray line is the normalized viscosity of the lower mantle (Mitrovica and Forte, 2004).

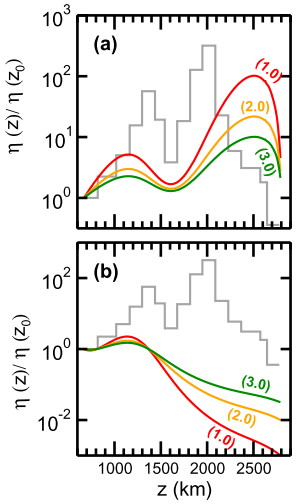

Fig. 4. (Color online.) Calculated normalized Fp viscosity as a function of depth along (a) adiabatic and (b) superadiabatic geotherms for a power law fluid. The results are computed considering $G^*(z_0) = 300$ kJ/mol and $\delta = 0.5$. The red, orange, and green lines represent n respectively 1, 2, and 3. The gray line is the normalized viscosity of the lower mantle (Mitrovica and Forte, 2004).

peradiabatic geotherm, the viscosity shows only one peak around 1200–1500 km depending on the value of δ.

Fig. 3 presents the normalized viscosity along the geotherms for several activation energies at the top of the lower mantle, $G^*(z_0)$, ranging from 200 to 500 kJ/mol, with $\delta = 0.5$ and $n = 1$. The results indicate that variations in the activation energy do not change qualitatively the viscosity profile. Fig. 4 presents the Fp viscosity along the geotherms if one considers Fp as a power law fluid (with $G^*(z_0) = 300$ kJ/mol and $\delta = 0.5$), as computed by the effective viscosity of an equivalent Newtonian fluid (Karato, 1981). The results show that variations in n do not affect considerably the undulations in the viscosity.

Changes in the elastic parameters due to iron spin transition of Fp causes dramatic variations in the rheological properties of the material. The results indicate that the observed viscosity undulations in the mid-lower mantle could be correlated to the spin transition in Fp. The viscosity hills in the mid-lower mantle have already been shown to exert effects on the dynamics of mantle plumes (Yuen et al., 1996), so that such plumes may have some connection with the spin transition occurring in the mantle. The low viscosity in mid mantle provides a region for chemical mixture of minerals. Therefore, the iron spin transition provides a new ingredient in mantle rheology and should be included in geodynamical modeling of the lower mantle.

4. Implications for mantle dynamics

Implications of the undulated lower mantle viscosity profile exist for both, down- and up-wellings in the mantle. Three dimensional models show that a viscosity "hill" of one order of magnitude through 500–1000 km of lower mantle is sufficient to slow down the sinking speed of a slab, and that a viscosity peak of two orders of magnitude can completely stop the sinking (Morra et al., 2010). Analytical calculations demonstrate that the sinking velocity of a slab is only weakly dependent on its geometry, and described by the rate $S[1 + \ln(L/S)]$ (Capitanio et al., 2007), where L and S are the two orthogonal maximum lengths, respectively. Approximating S as the size of the upper mantle (~1000 km), subducted lithospheres are expected to sink in the lower mantle at a speed inversely proportional to the mantle viscosity, regardless on the slab morphology. Recent estimations of sinking velocities based on matching plate reconstructions with mantle tomography confirmed this scenario averaging the slab sinking speed to 12 to 13 mm/yr (van der Meer et al., 2010; Butterworth et al., 2014).

Based on these elements, we suggest that the high velocity anomalies observed at 2000 km depth (Van der Hilst and Kárason, 1999) can be explained by the rheological variations due to the mid lower mantle spin transition. Mantle tomography shows that some of the largest slabs sink into the lowermost mantle while others stall, or are characterized by very long transient times. Morra et al. (2010) found a transition between sinking and stalling for a mantle profile model compatible with an adiabatic mantle model characterized by activation energies around $G^*(z_0)$ ~300–400 kJ/mol for a linear mantle viscosity (characteristic of diffusion creep) and dilation $\delta = 0.5$ or lower.

Following the procedure described in Section 2, we have modeled how the undulating mantle viscosity profile modifies the speed and size of a rising plume head. We assumed that its volume increases due to entrainment from the plume tail, as benchmarked by laboratory and numerical models (Griffiths and Campbell, 1990; Ribe et al., 2007). From the observation that the crossing time of the plume head through the high viscosity region is proportional to the mantle viscosity (from the rising speed $V = g\Delta\rho a^2/3\eta_0$), we predict a scaling increase of the plume head radius proportional to the square root of the mantle viscosity $a/a_0 = \sqrt{\eta_0}$. This implies that if the viscosity peak reaches two orders of magnitude above the average mantle, the linear size of the plume head will increase of one order of magnitude, and its volume of three orders of magnitude.

Our 1D approach, based on the approximated assumption of a spherical shape of the plume head, allows quantifying the relationship between plume head size and the intensity of the lower viscosity undulations. Fig. 5 shows the model results of the evolution of the plume head radius a, given by $\partial a/\partial t = \sqrt{a\kappa g\Delta\rho/6\eta_0}$ (see Section 2 for details), for six lower mantle viscosity profile (adiabatic and superadiabatic, $\delta = 0.0$, 0.5 and 1.0). For each mantle profile, we explored three families of ten time-evolution models. Each family is characterized by one value of average plume–mantle temperature difference ΔT (150 K, 300 K and 450 K). For each ΔT, we varied the initial plume radius a_0 from 50 km to 150 km, testing one model every 10 km. While we find that all superadiabatic mantle profiles, regardless on the dilation parameter δ, have a minor effect on the plume evolution, a plume crossing the undu-

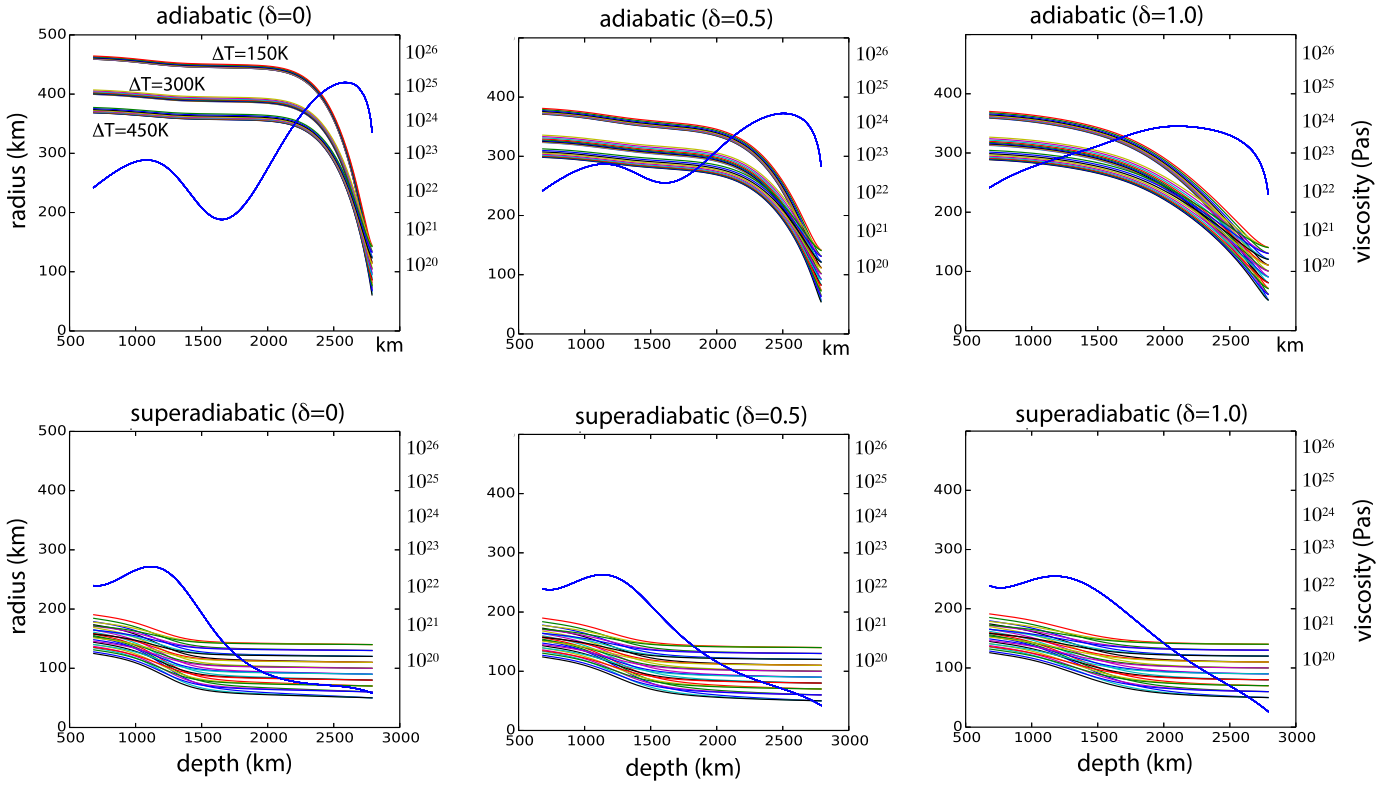

Fig. 5. (Color online.) Plume head radius (in km) vs. depth (in km) as obtained from the numerical integration of the entrainment plume head growth described in Section 2. The six plots refer to adiabatic and superadiabatic geotherms, $G^*(z_0) = 300$ kJ/mol, $n = 1$, for $\delta = 0.0$, 0.5 and 1.0. Three families of plot show the range of variation for three (assumed constant) differential temperature between the plume and the background mantle $\Delta T = 150$ K, 300 K and 450 K, as indicated by the labels. Ten lines represent the range of starting values of the head radius, ranging from 50 km (initial volume $V_0 \sim 5 \times 10^5$ km^3) to 150 km ($V_0 \sim 1.4 \times 10^7$ km^3). The plume head is assumed spherical at a first order, therefore the plot represents an upper bound for the volume. The blue line is the associated viscosity model. The plot shows how the size of the plume head is primarily controlled by the largest viscosity peak in the lower mantle, then by the differential density between the plume and the mantle, and does not show almost any dependency from the nucleation size.

lations of an adiabatic mantle displays instead a dramatic change of the plume head size (Fig. 5).

Our models show that the evolution of the plume head size for adiabatic profiles is dominated by the size of the greatest peak of the viscosity in the lower mantle, and to be up to two orders of magnitude (Fig. 5). The rising velocity is strongly modulated by both the greater and minor peak of the mantle viscosity fluctuations (Fig. 6). However, the larger peak has a primary control on the plume size, being the rising speed inversely proportional to the background viscosity. Because the period of entrainment is proportional to the time necessary to cross the high viscosity layer, the plume size is mostly dominated by the amplitude and thickness of the high viscosity region.

We find that the size of the initial plume radius, the nucleation of the plume, has a minimum effect to the size that the head reaches at the surface. A greater role is instead played by the average temperature difference between plume and mantle, that can change the final integrated radius of the plume of about 25%, equivalent to a duplication of the volume head, for a factor of three of increase of ΔT (from 150 K to 450 K).

The combination plume head size and velocity speed (Figs. 5 and 6) suggests that a dilation parameter $\delta = 0.0$ is too small, since the time necessary to overcome the high viscosity region is of the order of several hundreds of Myrs or greater. Instead, the integrated effect of the viscosity profile with $\delta = 0.5$ and $\delta = 0.0$ decreases rising time to less than 100 Myrs, compatible with the life length of deep mantle plumes. Our models show that only an undulated lower mantle viscosity profile is capable of producing plume heads characterized by a radius above 300 km. This corresponds to a surface extension of the order of 0.1–1.0 Mkm^2, compatible with the definition of Large Igneous Province that emerges from the most up-to-date databases (Bryan and Ernst, 2008).

Although our models are limited by the assumption of a spherical plume head, they capture the volumetric increase of the plume head in the range order of magnitude. Future 2D and 3D models will have to take into account the details of the plume dynamics and quantify more precisely the departure from the present 1-D analysis.

5. Summary

In summary, we have demonstrated that changes in the elastic parameters due to iron spin transition of Fp can produce dramatic variations in the rheological properties of the material, as to cause a non-monotonic behavior with depth. Our results indicate that, at lower mantle conditions, the effect of the spin transition in Fp is to create viscosity undulations respect to the radial profile and also horizontal variations. High viscosity regions would trap sinking slabs favoring chemical mixing, and that this picture concurs with mantle tomographic models (Van der Hilst and Kárason, 1999; Boschi et al., 2008). Complexities in the dynamics of mantle plumes are expected, such as the formation of large plume heads (e.g. Lin and van Keken, 2005). Since the inception of most plumes has been shown to be characterized by a Large Igneous Province (LIP), we propose that this dramatic size increase could be linked to their setting. Future models, in 2D and 3D, will have to explore the details of the plume evolution, going beyond the spherical assumption used here only to calculate the order of magnitude of the effect on lower mantle geodynamics. Therefore, we conclude that the iron spin transition provides a new ingredient in man-

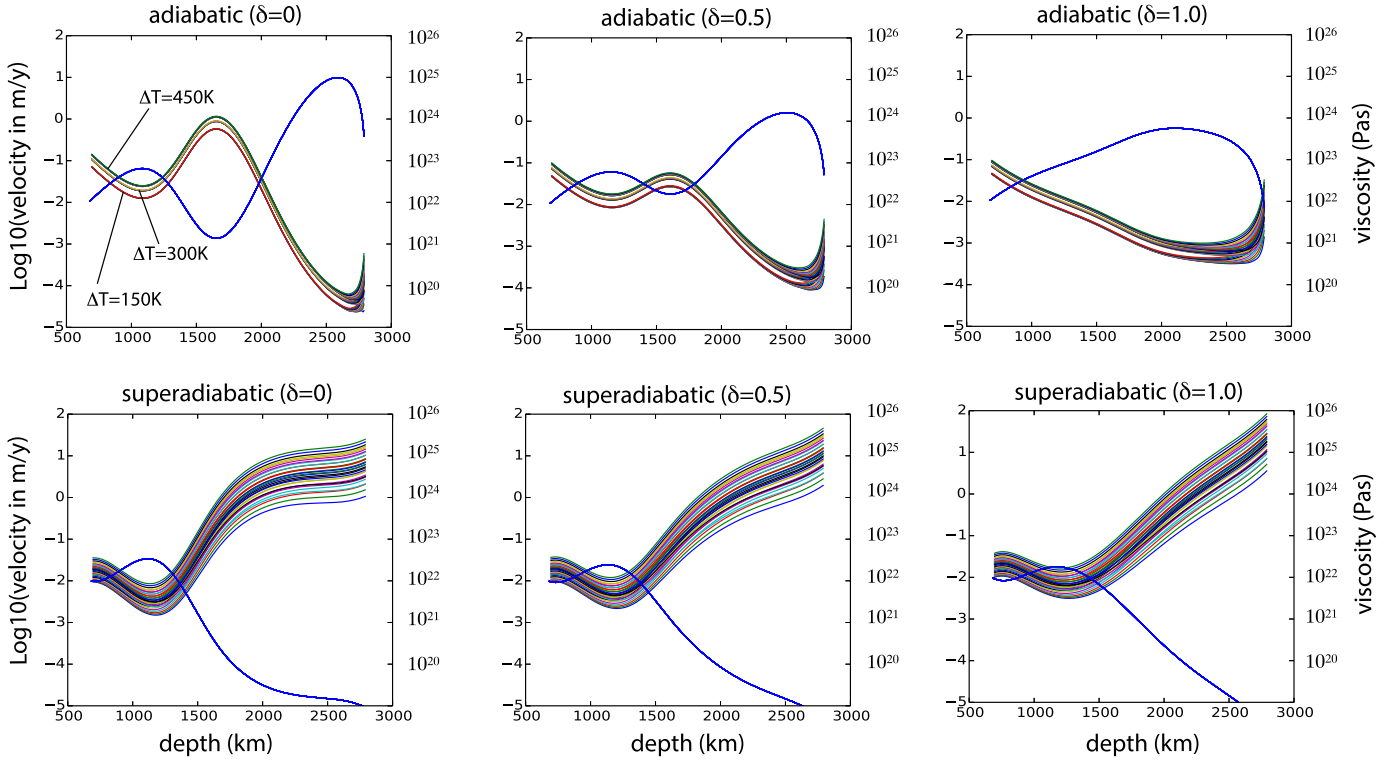

Fig. 6. (Color online.) Calculated rising speed in (in logarithmic scale) of the plume head from the core–mantle boundary to the surface. The results refer to the same models shown in Fig. 5 (adiabatic and superadiabatic geotherms, $G^*(z_0) = 300$ kJ/mol, $n = 1$ and $\delta = 0.0$, 0.5 and 1.0), three families for $\Delta T = 150$ K, 300 K and 450 K, the models for family $a_0 = 50$ km to 150 km, each 10 km. The plot shows that the rising speed mirrors the mantle viscosity profile. The greater the viscosity peak, the smaller is the difference between the profiles of the plume rising speeds, since the plume head emerges from the high viscosity region with similar size. The difference between model families (different ΔT) is a linear dependency between rising speed and differential density. The models show that although the plume head size changes minimally when crossing the second peak, the rising speed displays large variations, being inversely dependent on the background mantle viscosity.

tle rheology and should be included in future global geodynamic modeling.

Acknowledgements

This research was partially supported by grants NSF/EAR 0635990, NSF/ITR 0428774, and NSF/DMR 0325218 (ITAMIT) and the geochemistry and geophysics programs of the National Science Foundation. Computations were performed at the Minnesota Supercomputing Institute and on the Big Red Cluster at Indiana University. JFJ acknowledges partial support from Brazilian agencies FAPESP (grant number 2009/14082-3) and CNPq (grant number 473307/2013-8). GM acknowledges Louisiana Board of Regents – Research Competitiveness Subprogram LEQSF Grant (2014-17)-RD-A-14.

References

Antonangeli, D., Siebert, J., Aracne, C.M., Farber, D.L., Bosak, A., Hoesch, M., Krisch, M., Ryerson, F.J., Fiquet, G., Badro, J., 2011. Spin crossover in ferropericlase at high pressure: a seismologically transparent transition? Science 331, 64–67.

Badro, J., Fiquet, G., Guyot, F., Rueff, J.P., Struzhkin, V.V., Vankó, G., Monaco, G., 2003. Iron partitioning in Earth's mantle: toward a deep lower mantle discontinuity. Science 300, 789–791.

Badro, J., Rueff, J.P., Vankó, G., Monaco, G., Fiquet, G., Guyot, F., 2004. Electronic transitions in perovskite: possible nonconvecting layers in the lower mantle. Science 305, 383–386.

Boehler, R., 2000. High-pressure experiments and the phase diagram of lower mantle and core materials. Rev. Geophys. 38, 221–245.

Boschi, L., Becker, T.W., Steinberger, B., 2008. On the statistical significance of correlations between synthetic mantle plumes and tomographic models. Phys. Earth Planet. Inter. 167, 230–238.

Bryan, S., Ernst, R., 2008. Revised definition of large igneous provinces (LIPs). Earth-Sci. Rev. 86 (1–4), 175–202.

Butterworth, N.P., Talsma, A.S., Muller, R.D., Seton, M., Bunge, H.P., Schuberth, B.S.A., Heine, C., 2014. Geological, tomographic, kinematic and geodynamic constraints on the dynamics of sinking slabs. J. Geodyn. 73, 1–13.

Capitanio, F.A., Morra, G., Goes, S., 2007. Dynamic models of downgoing plate-buoyancy driven subduction: subduction motions and energy dissipation. Earth Planet. Sci. Lett. 262, 284–297.

Carrier, P., Justo, J.F., Wentzcovitch, R.M., 2008. Quasiharmonic elastic constants corrected for deviatoric thermal stresses. Phys. Rev. B 78, 144302.

Cococcioni, M., de Gironcoli, S., 2005. Linear response approach to the calculation of the effective interaction parameters in the LDA+U method. Phys. Rev. B 71, 035105.

Crowhurst, J.C., Brown, J.M., Goncharov, A.F., Jacobsen, S.D., 2008. Elasticity of (Mg, Fe)O through the spin transition of iron in the lower mantle. Science 319, 451–453.

da Silva, C.R.S., Wentzcovitch, R.M., Patel, A., Price, G.D., Karato, S.I., 2000. The composition and geotherm of the lower mantle: constraints from the elasticity of silicate perovskite. Phys. Earth Planet. Inter. 118, 103–109.

Ellsworth, K., Schubert, G., Sammis, C.G., 1985. Viscosity profile of the lower mantle. Geophys. J. R. Astron. Soc. 83, 199–213.

Fei, Y.W., Zhang, L., Corgne, A., Watson, H., Ricolleau, A., Meng, Y., Prakapenka, V., 2007. Spin transitions and equations of state of (Mg, Fe)O solid solutions. Geophys. Res. Lett. 34, L17307.

Forte, A.M., Mitrovica, J.X., 2001. Deep-mantle high-viscosity flow and thermochemical structure inferred from seismic and geodynamic data. Nature 410, 1049–1056.

Grand, S.P., 1994. Mantle shear structure beneath the Americas and the surrounding oceans. J. Geophys. Res. 99, 11591–11621.

Griffiths, R.W., Campbell, I.H., 1990. Stirring and structure in mantle starting plumes. Earth Planet. Sci. Lett. 99 (1–2), 66–78.

Ito, Y., Tomiuri, M., 2007. Pressure effect of self-diffusion in periclase (MgO) by molecular dynamics. J. Geophys. Res. 112, B04206.

Karato, S., 1981. Rheology of the lower mantle. Phys. Earth Planet. Inter. 24, 1–14.

Li, C., van der Hilst, R.D., Engdahl, E.R., Burdick, S., 2007. A new global model for P wavespeed variations in Earth's mantle. Geochem. Geophys. Geosyst. 9 (Q05018).

Lin, J.F., Struzhkin, V.V., Jacobsen, S.D., Hu, M.Y., Chow, P., Kung, J., Liu, H.Z., Mao, H.K., Hemley, R.J., 2005. Spin transition of iron in magnesiowüstite in the Earth's lower mantle. Nature 436, 377–380.

Lin, J.F., Vankó, G., Jacobsen, S.D., Iota, V., Struzhkin, V.V., Prakapenka, V.B., Kuznetsov, A., Yoo, C.S., 2007. Spin transition zone in Earth's lower mantle. Science 317, 1740–1743.

Lin, S.C., van Keken, P.E., 2005. Multiple volcanic episodes of flood basalts caused by thermochemical mantle plumes. Nature 436, 250–252.

Marquardt, H., Speziale, S., Reichmann, H.J., Frost, D.J., Schilling, F.R., 2009. Single-crystal elasticity of $(Mg_{0.9}Fe_{0.1})O$ to 81 GPa. Earth Planet. Sci. Lett. 287, 345–352.

Mitrovica, J.X., Forte, A.M., 2004. A new inference of mantle viscosity based upon joint inversion of convection and glacial isostatic adjustment data. Earth Planet. Sci. Lett. 225, 177–189.

Morra, G., Yuen, D.A., Boschi, L., Chatelain, P., Tackley, P., Koumoutsakos, P., 2010. The fate of the slabs interacting with a smooth viscosity discontinuity in the mid lower mantle. Phys. Earth Planet. Inter. 180, 271–282.

Morra, G., Yuen, D.A., Lee, S.M., Zhang, S., in press. Source of the Cenozoic volcanism in Central Asia. In: Morra, Yuen, King, Lee, Stein (Eds.), Subduction Dynamics. In: AGU Geophysical Monograph, vol. 211. AGU and Wiley publisher.

Panning, M.P., Romanowicz, B.A., 2006. A three dimensional radially anisotropic model of shear velocity in the whole mantle. Geophys. J. Int. 167, 361–379.

Peltier, W.R., Drummond, R., 2010. Deepest mantle viscosity: constraints from Earth rotation anomalies. Geophys. Res. Lett. 37, L12304.

Ribe, N., Davaille, A., Christensen, U., 2007. Fluid dynamics of mantle plumes. In: Mantle Plumes. Springer, Berlin, Heidelberg, pp. 1–48.

Ricard, Y., Wuming, B., 1991. Inferring the viscosity and the 3-d density structure of the mantle from geoid, topography and plate velocities. Geophys. J. Int. 105, 561–571.

Saha, S., Bengtson, A., Morgan, D., 2013. Effect of anomalous compressibility on Fe diffusion in ferropericlase throughout the spin crossover in the lower mantle. Earth Planet. Sci. Lett. 362, 1–5.

Sammis, C.G., Smith, J.C., Schubert, G., Yuen, D.A., 1977. Viscosity depth profile of Earth's mantle – effects of polymorphic phase-transitions. J. Geophys. Res. 82, 3747–3761.

Shahnas, M.H., Peltier, W.R., Wu, Z., Wentzcovitch, R., 2011. The high-pressure electronic spin transition in iron: potential impacts upon mantle mixing. J. Geophys. Res. 116 (B8), B08205.

Sigloch, K., McQuarrie, N., Nolet, G., 2008. Two-stage subduction history under North America inferred from multiple-frequency tomography. Nat. Geosci. 1 (7), 458–462.

Simmons, N.A., Forte, A.M., Grand, S.P., 2006. Constraining mantle flow with seismic and geodynamic data: a joint approach. Earth Planet. Sci. Lett. 246, 109–124.

Speziale, S., Milner, A., Lee, V.E., Clark, S.M., Pasternak, M.P., Jeanloz, R., 2005. Iron spin transition in Earth's mantle. Proc. Natl. Acad. Sci. USA 102, 17918–17922.

Stretton, I., Heidelbach, F., Mackwell, S., Langenhorst, F., 2001. Dislocation creep of magnesiowüstite $(Mg_{0.8}Fe_{0.2}O)$. Earth Planet. Sci. Lett. 194, 229–240.

Tsuchiya, T., Wentzcovitch, R.M., da Silva, C., de Gironcoli, S., 2006. Spin transition in magnesiowüstite in Earth's lower mantle. Phys. Rev. Lett. 96, 198501.

Van der Hilst, R.D., Kárason, H., 1999. Compositional heterogeneity in the bottom 1000 km of Earth's mantle: towards a hybrid convection model. Science 283, 1885–1888.

van der Meer, D.G., Spakman, W., van Hinsbergen, D.J., Amaru, M.L., Torsvik, T.H., 2010. Towards absolute plate motions constrained by lower-mantle slab remnants. Nat. Geosci. 3 (1), 36–40.

van Keken, P., Yuen, D.A., van den Berg, A., 1992. Pulsating diapiric flows: consequences of vertical variations in mantle creep laws. Earth Planet. Sci. Lett. 112 (1), 179–194.

Van Orman, J.A., Fei, Y.W., Hauri, E.H., Wang, J.H., 2003. Diffusion in MgO at high pressures: constraints on deformation mechanisms and chemical transport at the core–mantle boundary. Geophys. Res. Lett. 30, 1056.

Wentzcovitch, R.M., Justo, J.F., Wu, Z., da Silva, C.R.S., Yuen, D.A., Kohlstedt, D., 2009. Anomalous compressibility of ferropericlase throughout the iron spin cross-over. Proc. Natl. Acad. Sci. USA 106, 8447–8452.

Wu, Z., Justo, J.F., da Silva, C.R.S., de Gironcoli, S., Wentzcovitch, R.M., 2009. Anomalous thermodynamic properties in ferropericlase throughout its spin crossover transition. Phys. Rev. B 80, 014409.

Wu, Z., Justo, J.F., Wentzcovitch, R.M., 2013. Elastic anomalies in a spin-crossover system: ferropericlase at lower mantle conditions. Phys. Rev. Lett. 110, 228501.

Wu, Z., Wentzcovitch, R.M., 2014. Spin crossover in ferropericlase and velocity heterogeneities in the lower mantle. Proc. Natl. Acad. Sci. USA 111, 10468–10472.

Yamazaki, D., Karato, S., 2001. Some mineral physics constraints on the rheology and geothermal structure of Earth's lower mantle. Am. Mineral. 86, 385–391.

Yuen, D.A., Cadek, O., van Keken, P., Reuteler, D.M., Kyvalova, H., Schroeder, B.A., 1996. In: Boschi, E., Ekstrom, G., Morelli, A. (Eds.), Seismic Modelling of the Earth's Structure. Editrice Compositori, Bologna, Italy, pp. 463–506.

Zerr, A., Boehler, R., 1994. Constraints on the melting temperature of the lower mantle from high-pressure experiments on MgO magnesiowüstite. Nature 371, 506–508.